Title: Long chain n-3 fatty acids attenuate oncogenic KRas driven proliferation by altering plasma membrane nanoscale proteolipid composition

Authors and affiliations: Natividad R. Fuentes[1, 2], Mohamed Mlih[3], Rola Barhoumi[4], Yang-Yi Fan[1], Paul Hardin[5], Trevor Steele[6], Spencer Behmer[6], Ian A. Prior[7], Jason Karpac[3] and Robert S. Chapkin[1, 8]*.

[1]Program in Integrative Nutrition & Complex Diseases; [2]Department of Veterinary Physiology & Pharmacology; [3]Department of Molecular and Cellular Medicine, College of Medicine, Texas A&M Health Sciences Center; [4]Department of Veterinary Integrative Biosciences; [5]Department of Biology; [6]Department of Entomology; [7]Division of Cellular and Molecular Physiology, University of Liverpool; and [8]Center for Translational Environmental Health Research, Texas A&M University.

* To whom correspondence should be addressed, 111 Cater Mattil, Texas A&M University, College Station, TX, 77843, USA. Tel: 979-845-0419; Email: r-chapkin@tamu.edu

Running Title: n-3 PUFA modifies KRas nanoscale proteolipid composition

Keywords: n-3 PUFA, Plasma membrane, Oncogenic Ras, Colon, Diet

Additional information.

The authors declare no potential conflicts of interest.

Abstract

Approximately half of colorectal cancers are driven by activating mutations in KRas which confer resistance to standard therapies. Ras signalling originates from transient nanoscale compartmentalized regions of the plasma membrane composed of specific proteins and lipids. The highly specific lipid composition of these nanodomains, termed nanoclusters, facilitates effector recruitment, and therefore influences signal transduction. This suggests that Ras nanocluster proteolipid composition could represent a novel target for future chemoprevention interventions. There is evidence that the consumption of fish oil, containing long-chain n-3 polyunsaturated fatty acids (n-3 PUFA) such as eicosapentaenoic acid (EPA, $20{:}5^{\Delta 5,8,11,14,17}$) and docosahexaenoic acid (DHA, $22{:}6^{\Delta 4,7,10,13,16,19}$), may reduce colon cancer risk in humans, however the mechanism underlying this effect is unknown. We demonstrate that dietary n-3 PUFA, via their physical incorporation into plasma membrane phospholipids, reduce the lateral segregation of cholesterol-dependent and independent nanoclusters, and suppress phosphatidic acid-dependent oncogenic KRas effector interactions. This results in the attenuation of oncogenic Ras-driven colonic hyperproliferation in both *Drosophila* and murine models. These findings demonstrate the unique properties of dietary n-3 PUFA in the shaping of Ras nanoscale proteolipid complexes and support the emerging role of plasma membrane targeted therapies.

Introduction

Approximately 45% of colorectal cancers (CRCs) harbor KRas mutations[1], which confer resistance to standard therapy[2]. Moreover, to date, targeting of mutant Ras proteins in cancers has not been possible[3]. A number of Ras effector proteins and cell signaling pathways have been defined, including the Raf and the MAP kinase pathway, the PI3K and the Akt/mTOR pathway, and the RalGDS and Ral pathway. Ras effector proteins physically associate with Ras proteins to propagate signal transduction[4]. These signals result in increased proliferation, decreased apoptosis, disrupted cellular metabolism, and increased angiogenesis, all seminal hallmarks of cancer[5]. Thus, there is a critical need to develop new KRas targeted therapeutic approaches with reduced toxicities in the setting of acute or chronic administration.

High fidelity signaling of KRas is dependent on its spatial organization into defined proteolipid nanoassemblies[6]. Recently, it was demonstrated that select amphiphilic agents, through direct modulation of the biophysical properties of the plasma membrane, compromise oncogenic KRas mediated signal transduction by altering its precise nanoscale membrane organization[7]. Furthermore, the paradoxical activation of MAPK signaling by BRaf inhibitors in oncogenic KRas expressing cells is driven by an increase in KRas nanoassembly clustering[8]. These findings suggest that Ras nanoscale proteolipid composition could be a novel therapeutic target[8].

The molecular mechanisms that influence the formation and structure of Ras nanoclusters involve lipid-lipid and protein-lipid interactions between the C-terminal plasma membrane anchor and plasma membrane phospholipids[9]. In regard to membrane phospholipids, recent work has shown that nanocluster formation is not only dependent on the charged head groups[10], but also the asymmetry and saturation index of the fatty acyl

lipid tail region[11]. Interestingly, dietary consumption of long-chain n-3 polyunsaturated fatty acids (n-3 PUFA), such as eicosapentaenoic acid (EPA, $20{:}5^{\Delta 5,8,11,14,17}$) and docosahexaenoic acid (DHA, $22{:}6^{\Delta 4,7,10,13,16,19}$), results in the incorporation of these fatty acids into cell membrane phospholipids[12]. This is noteworthy because the consumption of EPA and DHA may reduce colon cancer risk in humans[13]. Hence, establishing a causal role of n-3 PUFA in colon cancer prevention would have a major translational impact because these dietary nutrients are relatively inexpensive, safe and well tolerated[14]. However, the molecular mechanisms by which n-3 PUFA specifically impact oncogenic KRas-driven colon cancer remain to be determined. Herein, we report that the incorporation of DHA and EPA into plasma membrane phospholipids (i) modifies KRas nanoscale proteolipid composition, (ii) disrupts oncogenic KRas driven signaling (pERK), and (iii) suppresses KRas associated phenotypes (hyperproliferation) *in vitro* and *in vivo*. Together, these results suggest a unique role for n-3 PUFA in the modulation of KRas nanoscale spatial organization and signaling.

Material and Methods

Mouse genetics, husbandry and diet.

The animal use protocol was approved by the University Animal Care Committee of Texas A&M University and conformed to NIH guidelines. To generate an inducible colonic targeted oncogenic KRas mouse model, CDX2P-CreERT2 mice (RRID:IMSR_JAX:022390) were crossed with LSL-K-ras G12D mice (RRID:IMSR_JAX:008179). Mice were housed in cages in a temperature- and humidity-controlled animal facility with a 12 h light/dark cycle and fed lab chow.

For *in vivo* diet studies, mice were fed experimental diets containing either n-6 (control) or n-3 PUFA for two weeks prior to tamoxifen injection (**Figure 1A**). Both diets contained 20% (w/w) casein, 42% sucrose, 22% cornstarch, 6% cellulose, 3.5% AIN-76 mineral mix, 1% AIN-76 vitamin mix, 0.3% methionine, 0.2% choline, and 0.02% tert-Butylhydroquinone (TBHQ). The n-6 diet contained 5% (w/w) corn oil (Dyets, Bethlehem, PA, #401150), and the n-3 diet contained 4% menhaden fish oil (Omega Pure, Houston, TX) and 1% corn oil. The diets were changed daily and contained TBHQ in order to prevent peroxidation. Four weeks prior to termination, mice were injected once intraperitoneally (i.p.) with 200 mg/kg tamoxifen (Sigma-Aldrich, # T5648)[15] dissolved in corn oil (as a carrier) or injected with corn oil alone.

In Vivo Measurement of Crypt Proliferation and Length

For the purpose of measuring rates of colonic cell proliferation, mice were injected i.p. with 50 mg/kg EdU (Life Technologies, #A10044) 2 h prior to termination. At the time of euthanasia, colon tissue was flushed with PBS and the colon was processed to generate Swiss rolls[16]. Swiss rolls were subsequently fixed in 4% paraformaldehyde and embedded in paraffin. For cell proliferation assays, formalin-fixed paraffin-embedded 4 μm colon Swiss roll sections were deparaffinized and rehydrated through graded ethanol washes. Cell proliferation in colonic

crypts was measured using the Click-iT EdU Alexa Fluor 555 Imaging kit (Life Technologies, #C10338) as per the manufacturer's instructions[16]. Negative control slides were incubated without Alexa Fluor.

For crypt length, tissue sections were stained with Alcian blue and imaged with a Leica Aperio CS2 digital pathology scanner. Crypt measurement was performed using ImageScope (RRID:SCR_014311) software.

Cell Culture

Conditionally immortalized Young Adult Mouse Colonic (YAMC) cells (RRID:CVCL_6E40) were originally obtained from R.H. Whitehead, Ludwig Cancer Institute (Melbourne, Australia). YAMC cells (passages 14–20) were cultured under permissive conditions, 33°C and 5% CO_2 in RPMI 1640 media (Mediatech, Manassas, VA) supplemented with 5% fetal bovine serum (FBS; Hyclone, Logan, UT), 2 mM GlutaMax (Gibco, Grand Island, NY), 5 μg/mL insulin, 5 μg/ml transferrin, 5 ng/ml selenious acid (Collaborative Biomedical Products, Bedford, MA), and 5 IU/mL of murine interferon-γ (Roche, Mannheim, Germany). YAMC cells were authenticated (07/24/15) by STR profiling (CellCheck Plus) by IDEXX BioResearch (Westbrook, Maine). Isogenic SW48 KRas (G12D/+) cells (RRID:CVCL_LC92) were obtained (10/08/14) from Horizon Discovery (Cambridge, United Kingdom), where they were authenticated by gDNA and cDNA genotyping. SW48 cells (passages 8-13) were maintained at 37°C and 5% CO_2 in McCoy's 5A medium supplemented with 10% FBS. DKOB8 cells were acquired (09/19/03) from Dr. Patrick Casey (Duke University) who maintained them for Dr. Gideon Bollag, Onyx-Pharmaceuticals (San Francisco, California)[17]. DKOB8 cells (passages 7-12) were maintained at 37°C and 5% CO_2 in Dulbecco's Modified Eagle Medium, high glucose medium supplemented with 5% FBS. Where indicated, DKOB8 cells were incubated with 10 μM ponasterone A (ThermoFisher, H10101) for 48 h, which verifies the cell type by large induction

of KRas. All cell lines used tested negative for mycoplasma bacteria (09/15/16) as assessed by a MycoAlert PLUS Mycoplasma Detection Kit (Lonza, #LT07-701). Select cultures were treated for 72 h with 50 μM fatty acid [linoleic acid (LA, 18:2n6), arachidonic acid (AA, 20:4n6), eicosapentaenoic acid (EPA, 20:5n3) or docosahexaenoic acid (DHA, 22:6n3); NuChek, Elysian, MN] complexed with fatty acid free bovine serum albumin (BSA).

Drosophila genetics, stocks, and culture.

The following strains were obtained from the Bloomington *Drosophila* Stock Center: w1118, UAS-Ras^{V12} (BDSC Cat# 64196, RRID:BDSC_64196), and tub-Gal80ts (DGGR Cat# 130454, RRID:DGGR_130454). esg-Gal4 was kindly provided by Dr. Shigeo Hayashi, Riken Center for Developmental Biology. UAS-GFP-tK, UAS-RFP-tK, UAS-GFP-tH, UAS-RFP-tH were kindly provided by Dr. John F. Hancock, University of Texas Health Science Center - Houston[18]. All flies were reared on Bloomington's standard medium at 25°C and 65% humidity on a 12h light/dark cycle, unless otherwise indicated. Newly emerged flies were transferred into vials with the test diets and maintained for 5 days.

Drosophila Holidic Diet

A holidic diet was prepared as previously described[19]. Briefly, individual diet components were mixed and prepared in a gel form with agar. Once the diet cooled to < 60ºC, corn oil (1.79% w/w) or fish oil (1.79% w/w) along with TBHQ (0.02% w/w) was added and the diet was vigorously shaken to ensure uniform mixing, prior to decanting into plastic feeding tubes. The fatty acid composition of the diets is described in **Supplemental Table 4.** Newly emerged adult female flies were transferred to diets for 5 days prior to dissection and the collection of their guts for lipid profiling and imaging. Dietary fish oil was well tolerated, which is consistent with previous studies, demonstrating that dietary long-chain fatty acids are tolerated and readily incorporated into larvae, pupae and adult fly membrane lipids[20,21].

Conditional Expression of UAS-Linked Transgenes

The esgGal4 driver was combined with a ubiquitously expressed temperature-sensitive Gal80 inhibitor (tubGal80ts). The escargot construct drives expression in stem cells using the EGFR-Ras axis to maintain stemness and suppress differentiation[22]. Crosses and flies were kept at 18°C (permissive temperature) and 5-day-old females were fed the test diets 5 days and then shifted to 29°C for 2 days to allow expression of the transgenes before analysis.

***Drosophila* Immunostaining and Microscopy**

Intact fly guts were fixed at room temperature for 20 min in 100 mM glutamic acid, 25 mM KCl, 20 mM $MgSO_4$, 4 mM sodium phosphate, 1 mM $MgCl_2$, and 4% formaldehyde. All subsequent incubations were performed using PBS, 0.5% BSA, 0.1% Triton X-100 at 4°C. The following primary antibodies were used: anti-phospho-Histone H3 (Millipore; 1:1000), anti-armadillo (1:250 dilution), obtained from the Developmental Studies Hybridoma Bank. Fluorescent secondary antibodies were obtained from Jackson ImmunoResearch. Hoechst dye was used to stain DNA. Confocal images were collected using a Nikon Eclipse Ti confocal system and processed using Nikon software and Adobe Photoshop.

Cell Line Immunofluorescence

For quantitative phospho-ERK analysis, cells were seeded in cell imaging 8 chamber coverglass slides (Eppendorf, 0030742036) and treated with select fatty acids (50 µM) for 72 h. Cells were subsequently serum starved (0% FBS) for 18 h in the presence of fatty acid, stimulated with EGF (25 ng/ml) (PeproTech, 315-09) for 5 min and immediately fixed in ice cold 100% methanol. Cells were incubated with primary phosphor-ERK (Cell Signaling Technology, #4370, 1:200, RRID:AB_2315112) antibody followed by alexa-647 fluorescent secondary antibody (Jackson ImmunoResearch Labs, #711-605-152, 1:400, RRID:AB_2492288).

CellMask™ Green Plasma Membrane Stain (ThermoFisher, #C37608, 1:1000) was used to label the cells and Hoechst 33342 (ThermoFisher, #H3570, 1:2000) to label the nucleus. Cells were imaged with a 1.3 numerical aperture 40x Plan-Fluor oil objective or 1.4 numerical aperture 100x Plan-Apo oil objective mounted on a wide field Nikon Eclipse microscope using identical settings between samples. For analysis, images were opened in NIH ImageJ software (ImageJ, RRID:SCR_003070; Fiji, RRID:SCR_002285), converted to Tiff files and a custom macro was used to quantify average fluorescent intensity of pERK. Briefly, green membrane stain was used to define a binary cell mask that was applied to pERK images. Average fluorescent intensity of the mask images was subsequently recorded (**Supplemental Figure 3**).

For quantitative nuclear pERK to cytoplasmic ratio analysis, images were captured with a 1.15 numerical aperture 40x ACS-Apo oil objective mounted on a Leica DMi8 TCS SPE spectral confocal microscope. After the nuclei were highlighted by Hoechst 33342 (ThermoFisher, #H3570), NIH ImageJ software (ImageJ, RRID:SCR_003070; Fiji, RRID:SCR_002285) was used to manually define the cytoplasm and nuclear fields of interest. Average intensities were used to quantify the nuclear to cytoplasm ratio.

Western Blot Analysis of Intestinal Proteins

For DKOB8 cell Western blotting, cells were homogenized in ice-cold homogenization buffer (50 mM Tris-HCl, pH 7.2, 250 mM sucrose, 2 mM EDTA, 1 mM EGTA, 50 mM sodium fluoride, 1%Triton X-100, Halt Phosphatase Inhibitor Cocktail (ThermoFisher, #78420), Protease Inhibitor Cocktail (Sigma, #P8340), and 10 mM β-mercaptoethanol. Following homogenization, lysates were sheared using a 29G needle, incubated on ice for 30 min, and centrifuged at 16,000 x *g* for 20 min. The supernatant was collected and protein concentration was assessed using Coomassie Plus Protein assay (Pierce, #23236). For each sample, 10 µg of protein lysate was treated with 4X Laemmli Sample Buffer (Bio-Rad, #161-0747) and subjected to SDS

polyacrylamide gel electrophoresis (PAGE) in precast 4–20% Mini-PROTEAN TXG Stain-Free Gels (Bio-Rad, #456-8096). After electrophoresis, total protein was activated and visualized with a ChemiDoc Imaging system (Bio-Rad, #17001401) according to manufactures instructions. Subsequently, proteins were electroblotted onto a nitrocellulose membrane with the use of a Trans-Blot Turbo Transfer Pack (Bio-Rad, #1704158) and Trans-Blot Turbo Transfer System (Bio-Rad, #1704150) according to manufacturer's instructions. Following transfer, total protein was visualized and the membrane was incubated in Membrane Blocking Solution (ThermoFisher, #000105) at room temperature for 1 h with shaking, followed by incubation with shaking overnight at 4^{o}C with primary antibody diluted in Membrane Blocking Solution. Membranes were washed with 0.1% Tween 20 in TBS (TBST) and incubated with secondary peroxidase conjugated secondary antibody as per manufacturer's instructions. Bands were developed using Clarity Western ECL substrate (Bio-Rad, #170-5060). Blots were visualized using a ChemiDoc Imaging System. Antibodies directed against phospho-ERK (Cell Signaling Technology, #4370; 1:2,000, RRID:AB_2315112), total ERK (Cell Signaling Technology, #4695; 1:1,000, RRID:AB_390779), and Pan-Ras (MilliporeSigma, #OP40; 1:1,000 dilution, RRID:AB_213400) were used. Peroxidase conjugated antibodies goat anti-rabbit IgG (Kirkegaard and Perry Laboratories, #074-1516; 1:20,000) and peroxidase conjugated goat anti-mouse IgG (Kirkegaard and Perry Laboratories, #074-1806; 1:20,000) were used.

For *Drosophila* western experiments, intact female guts were dissected in cold PBS and proteins extracted in Laemmli buffer, separated on 10% acrylamide gel and transferred according to standard procedures. Antibodies directed against phospho-ERK (Cell Signaling Technology, #4370; 1:1,000), total ERK (Cell Signaling Technology, #4695; 1:1,000), β-actin (Cell Signaling Technology; 1:5,000 dilution, RRID:AB_10950489) were used. Total protein extracts were pooled from 4 guts.

Fluorescence lifetime imaging microscopy combined with fluorescence resonance energy transfer (FLIM-FRET).

For *in vitro* FLIM experiments, YAMC cells were seeded at a density of $1x10^4$ in cell imaging 8 chamber coverglass (Eppendorf, 0030742036) 24 h prior to fatty acid-BSA (50 µM) treatment. Following a 24 h incubation period, media without fatty acid was added and Lipofectamine 3000 (ThermoFisher, #L3000-008) was used to transiently transfect cells with plasmids of donor (GFP-tagged protein) alone or co-transfected with FRET acceptors[7,18]. FRET acceptors were RFP-tagged proteins of interest (GFP-: RFP-plasmid at 1:3 ratio, 0.25 µg total plasmid per well). After 8 h in transfection media, cells were gently washed with PBS and incubated with complete media plus fatty acids for 40 h. Subsequently, cells expressing GFP-tagged protein alone or co-expressing both GFP-tagged and RFP-tagged proteins were washed with PBS and fixed in 4% PFA for 15 min. After three washes in 1X PBS, HPBS was added to wells. The GFP fluorescence lifetime was measured using a Lambert Instrument (Roden, The Netherlands) FLIM unit attached to a wide field Nikon Eclipse microscope. GFP was sinusoidally excited by a modulating 3-Watt 497 nm light-emitting diode (LED) at 40 MHz under epi-illumination. A solution of fluorescein (1 µM) was used as a lifetime reference standard. Cells were imaged with a 1.3 numerical aperture 40x Plan-Fluor oil objective using an appropriate GFP filter set. The phase and modulation were determined from 12 phase settings using the manufacturer's software. This analysis results in an image where the fluorescence lifetime of GFP is determined and assigned to each pixel. The color scale on each pixel represents the fluorescent lifetime, which equates to the level of interaction between the GFP and RFP tagged proteins. Lifetime (phase) values were pooled and averaged from regions of interest drawn on individual cells. Each experiment was replicated at least 2 times. Statistical analysis was performed using one-way ANOVA. The FLIM-FRET method is highly favored over intensity based FRET measurements because fluorescent lifetime is an intrinsic property of the

fluorescent molecule and is generally insensitive to weak signal, excitation source, and variations in the donor-acceptor ratio[23].

For *Drosophila* FLIM experiments, adult flies expressing GFP/RFP constructs in gut stem cells were dissected in PBS and fixed 20 min in 4% PFA prior to mounting in Mowiol medium. Fields of view were scanned with an inverted LSM 780 microscope (Carl Zeiss Microimaging, Thornwood, NY) and a 1.4 numerical aperture 40× Plan Apochromat oil objective. Two-photon excitation was provided by a Chameleon (Coherent Inc.) Ti:sapphire laser tuned to 900 nm. Emission events were registered with FastFLIM system (ISS, Champaign, IL). Fluorescence lifetime images (256 × 256 pixels) were acquired with a pixel dwell time of 6.3 µs. Lifetime of the imaged samples was determined with the frequency domain technique using the ISS VistaVision Suite version 4.1. At least 10 images were collected per treatment.

The percentage of the apparent FRET efficiency (E_{app}) was calculated using the measured lifetimes of each donor-acceptor pair (τ_{DA}) and the average lifetime of the donor only (τ_D) samples. The formula employed was $Eapp = (1-\tau_{DA}/\tau_D) \times 100\%$[24].

Lipid extraction and fatty acid analysis

For assessment of dietary lipid incorporation into membrane phospholipids, total lipids were extracted from isolated mouse crypts[25] and at least 28 dissected *Drosophila* guts per treatment with 2:1 (v/v) chloroform-methanol as previously described[26]. Total phospholipids were subsequently separated by thin-layer chromatography with 90:8:1:0.8 (v/v/v/v) chloroform-methanol-acetic acid-water. After transesterification using methanolic HCl, fatty acid methyl esters were quantified by capillary gas chromatography-mass spectrometry[26].

Lipid Add-Back

18:0-18:1 phosphatidic acid (#840861, 10 mg/mL in chloroform) and 18:0-18:1 phosphatidylserine (#840039, 10 mg/mL in chloroform) were obtained from Avanti Polar Lipids, dried under nitrogen gas, resuspended in 10 mM in 150 mM NaCl and 10 mM Tris·HCl, pH 8, immediately added to cultures at 100 μM final concentration and incubated for 45 min prior to cell fixation.

Results

Dietary n-3 PUFA ameliorate oncogenic KRasG12D mediated colonic phenotypes *in vivo*.

We previously demonstrated that n-3 PUFA suppress intestinal wild type Ras activation both *in vitro* and *in vivo*, by upstream disruption of epidermal growth factor receptor (EGFR) function[25,27]. However, oncogenic Ras contains a mutation that essentially keeps it in the active GTP-bound state[1], which renders it insensitive to upstream EGFR inhibition by anti-EGFR therapies[3]. To determine if dietary n-3 PUFA can suppress oncogenic Ras mediated colonic phenotypes, we utilized an inducible genetic model of oncogenic KRas driven colonic hyperproliferation targeted to the colon[15] (**Figures 1A**). Following tamoxifen injection, Cre-mediated recombination targeted to the epithelium of the distal ileum, cecum, colon and rectum removes transcriptional stop elements, resulting in expression of the mutant KRas allele under the control of its endogenous regulatory elements[15]. Mice were fed a diet containing corn (n-6 PUFA control) or fish oil, containing EPA and DHA (**Supplemental Tables 1 & 2**) for 2 weeks prior to tamoxifen induction of oncogenic KRas, and maintained for an additional 4 weeks (**Figure 1A**). Corn oil contains linoleic acid (LA, $18:2^{\Delta 9,12}$) which serves as a control for the non-specific effects of PUFA. The fish oil dose is comparable to a diet containing approximately 8.6 g/day n-3 PUFA in humans[28]. We have previously demonstrated that this dose is well tolerated and mice exhibit no signs of toxicity[25]. As expected, mice fed a diet containing n-3 PUFA exhibited an enrichment of EPA and DHA in membrane phospholipids (**Figure 1B and Supplemental Table 3**). Dietary n-3 PUFA treatment substantially reduced the colonic hyperproliferation induced by oncogenic KRas, as indicated by the significant ($P<0.05$) reduction of crypt length (**Figures 1C & E**) and number of EdU positive proliferative cells per crypt (**Figures 1D & F**). Collectively, these findings demonstrate

that dietary fish oil containing EPA and DHA can attenuate oncogenic KRas driven colonic phenotypes *in vivo*.

Long chain n-3 PUFA reshape plasma membrane nanoscale organization of cholesterol dependent and independent nanoclusters.

Previous experiments conducted by our lab using immuno-gold electron microscopy of plasma membrane sheets suggest that plasma membrane organization of inner leaflets is fundamentally altered by EPA and DHA[29,30]. Specifically, n-3 PUFA treatment altered the nanoscale organization of cholesterol-dependent (tH) and cholesterol independent (tK) probes expressed in cervical adenocarcinoma (HeLa) and colorectal carcinoma (HCT-116) cells[29,30]. These probes are composed of a fluorescent tag attached to the minimal membrane anchor of HRas (tH-GFP) or KRas (tK-RFP), which targets them to their respective membrane domains[31]. In the present study, we monitored the nanoscale organization of cholesterol sensitive (tH) and insensitive (tK) probes by fluorescence lifetime imaging combined with fluorescence resonance energy transfer (FLIM-FRET) microscopy[9]. When co-expressed with a corresponding FRET pair, such as RFP, a reduction of GFP lifetime is indicative of more extensive FRET as a result of a smaller distance between GFP and RFP, which is correlated with more extensive nanoclustering (**Figure 2A**). Lifetime values were then converted to apparent FRET efficiency %, where an increase is indicative of enhanced nanoclustering[24]. Importantly, transient expression of these probes faithfully reports on their fraction in nanoclusters, as this remains constant over a multi-log range of expression levels[6]. To explore the effects of n-3 PUFA on cholesterol-dependent and independent nanoclustering, we utilized immortalized young adult mouse colonocyte (YAMC) cells, which express wild type Ras. This model faithfully recapitulates n-3 PUFA *in vivo* effects[25,27,32] and allows for lipidomic and proteomic studies under well-controlled conditions[33]. Cells were treated with a physiologically relevant level (50 μM)[34] of albumin-complexed n-3 PUFA (EPA, DHA) or

control long-chain n-6 PUFA linoleic acid (LA) for 72 h. BSA-complexed fatty acids were used to represent the non-esterified fatty acids that are bound to albumin *in vivo*. We have previously demonstrated that this dose is well tolerated and cells exhibit no signs of toxicity[32]. In addition, mevastatin, an HMG-CoA inhibitor was used as a positive control to reduce nanoclustering of Ras and FRET efficiency by blocking farnesylation and thus membrane anchorage of Ras[24]. Interestingly, n-3 PUFA significantly increased ($P<0.05$) the clustering of tK-GFP (**Figures 2B & C**) while tH-GFP (**Figures 2D & E**) clustering was reduced ($P<0.05$) compared to untreated control. Since a reduction in FRET can result from disruption of Ras membrane nanoclustering as well as loss of membrane attachment[24], it is noteworthy that the plasma membrane association of tH-GFP but not tK-GFP is reduced following n-3 PUFA treatment[33].

n-3 PUFA are known to modulate differences in membrane rigidity between cholesterol-rich functional microdomains (lipid raft) and non-raft domains[35], thus we sought to determine if EPA and/or DHA could alter the lateral segregation of normally spatially separated cholesterol-dependent (tH-GFP) and independent (tK-GFP) nanoclusters. This outcome would result in the formation of mixed heterotypic nanoclusters, as observed with certain nonsteroidal anti-inflammatory drugs[7]. Interestingly, EPA and DHA significantly increased ($P<0.05$) the formation of heterotypic clustering, as did LA to a lesser extent (**Figures 2F & G**). Since the precise nanoscale organization of the minimal membrane anchor of KRas does not completely reflect the localization of its full length oncogenic constitutively activated counterpart[31,36], we performed similar heteroclustering experiments with the clinically relevant full-length form of oncogenic KRas. Our results show that EPA and DHA significantly increased the formation of full length oncogenic KRas and truncated HRas heteroclusters. In contrast, the n-6 PUFA control (LA) had no significant effect (**Figures 2H & I**). Taken together, these data demonstrate that the incorporation of n-3 PUFA into plasma membrane

phospholipids reshapes the nanoscale organization of cholesterol-dependent and independent nanoclusters, contributing to the generation of mixed nanoclusters of proteins that are normally segregated and spatially distinct.

Long chain n-3 PUFA attenuate oncogenic KRas mediated ERK signaling.

We next determined the functional consequences of n-3 PUFA induced nanoscale reorganization of the plasma membrane by examining oncogenic Ras-dependent signaling. For this purpose we utilized a human colon cancer SW48 cell line expressing mutated KRas. To limit the confounding effects associated with over-expression of oncogenic Ras[37], these cells were designed to express one copy of the mutated KRas variant G12D from the endogenous KRas locus. This particular KRas variant was chosen because one third of colorectal tumors harbor KRas mutations and ~80% of these mutations are at codon 12, while the remaining mutations are at codon 13[38]. Since physiological expression of oncogenic KRas does not result in large increases in phosphorylation of ERK, we opted to stimulate cells with EGF[37]. Incubation with EPA and DHA in comparison to untreated control reduced ($P<0.05$) EGF induced ERK phosphorylation by ~21 and 33%, respectively (**Figures 3A & B**). In contrast, the n-6 PUFA control (LA) had no effect compared to untreated control (**Figure 3B**).

To ensure that the observed effect of n-3 PUFA reducing pERK levels was directly caused by disruption of Ras signaling and not an upstream modulator such as EGFR[27], we utilized an oncogenic KRas inducible cell line, DKOB8. These cells were generated by replacing the original mutated KRas allele in DLD-1 cells with a mutated KRasG12D allele under the control of the ecdysone-inducible vector system[17]. This system allows for conditional expression of oncogenic KRas in the presence of ponasterone A, an analog of the insect steroid ecdysone (**Supplemental Figure 1**). Cells incubated with ponasterone A with and without fatty acid

treatment exhibited an increase in pERK in the DKOB8 KRasG12D overexpression model as determined by immunofluorescence (**Figures 3C & D**) and western blot (**Supplemental Figure 1**). Since translocation of pERK from the cytoplasm to the nucleus is required for mitogen induced cell proliferation[39,40], in complementary experiments, ERK activation and location was assessed by determining the ratio of active pERK in the nucleus vs the cytoplasm using quantitative immunofluorescence (**Figure 3E)**. DHA and EPA reduced ($P<0.05$) oncogenic KRas driven nuclear pERK accumulation in the DKOB8 model as compared to untreated and n-6 PUFA treated (LA) cells (**Figure 3E & F**).

Dietary n-3 PUFA reshape the nanoscale organization of sterol-dependent and independent nanoclusters and suppress oncogenic Ras-mediated hyperproliferation in *Drosophila* intestinal stem cells.

It is widely reported that a disconnect can occur between cell culture and *in vivo* systems. This is an especially challenging problem in the fields of cancer biology and nutrition, where complex cellular interactions govern the phenotypic outcome. To resolve this inconsistency, we further examined the membrane altering properties of n-3 PUFA on functional phenotypic and mechanistic Ras clustering outcomes *in viv*o. For this purpose, we utilized the *Drosophila* intestinal (midgut) epithelium model. The presence of somatic intestinal stem cells (ISCs) within the fly midgut allows for the use of a wide range of genetic tools to assay signalling events that govern proliferative homeostasis *in vivo*[41]. This barrier epithelia, with functional and morphological similarities to the mammalian small intestine and mouse airway epithelia[41], contains ISCs that can asymmetrically divide, forming an enteroblast (EB) that directly differentiates into functional enterocytes (**Figure 4A**). Thus, the *Drosophila* ISC lineage provides an excellent model to study signaling mechanisms regulating stem cell maintenance and dysfunction, including Ras-mediated proliferative signaling[41,42].

Initially, to extend our findings in YAMC cells, we assessed the effects of a fish oil-enriched diet containing n-3 PUFA on sterol-dependent and independent nanoclusters in *Drosophila* utilizing transgenic flies that express Ras FRET pair constructs (UAS-GFP/RFP-truncated KRas and/or UAS-GFP/RFP-truncated HRas)[18] specifically within ISCs/EBs (using the EsgGal4 driver). Similar to previous *in vitro* cell culture experiments, control flies expressing only the UAS-GFP-truncated KRas/esgGal4 stem cell driver (lacking the FRET pair; establishes baseline lifetime of GFP with no FRET interaction) or UAS-GFP/RFP-truncated HRas/esgGal4 (used to comparatively determine treatment effects on clustering of truncated HRas) were also assessed. Flies were fed a chemically defined holidic diet[19] that allowed for precise control over all ingredients. The experimental diet differed from the control diet only in its lipid profile – fish oil at 1.79% (w/w) (**Supplemental Table 4**). Phospholipid analysis of the midgut indicated that EPA, and to a lesser extent DHA, was enriched in flies feeding on the n-3 PUFA-enriched diet (**Table 1**). Utilizing these dietary and genetic conditions, we then performed FLIM-FRET to monitor truncated H- and KRas nanoclustering in *Drosophila* intestinal stem cells/enteroblasts. Consistent with our *in vitro* nanoclustering data (**Figures 2B-G**), flies on the fish oil diet had increased tK clustering, reduced tH clustering and increased formation of heterotypic clustering (**Figure 4B-E**). In a complementary set of experiments, flies were fed an additional n-6 PUFA control diet containing equal amounts of lipid (corn oil) (**Supplemental Table 4**). This resulted in a dramatic increase in LA-containing phospholipids (**Supplemental Table 5**), however no effect on tK or tH clustering was observed (**Supplemental Figure 2**). Finally, we examined the effect of dietary n-3 PUFA on oncogenic Ras-mediated phenotypes originating from stem cells in the *Drosophila* midgut. For this purpose, the expression of oncogenic RasV12 was targeted to ISCs in the adult fly, which leads to stem cell hyperproliferation and intestinal dysplasia (**Figure 4F**)[42]. Flies fed n-3 PUFA vs control exhibited a reduction in stem cell hyperproliferation, luminal thickening/tissue dysplasia (**Figures 4F-G**) and ERK activation (**Figure 4H**). Collectively,

these data demonstrate that dietary fish oil results in the incorporation of n-3 PUFA into plasma membrane phospholipids in *Drosophila* midguts, which is associated with the reshaping of sterol-dependent and independent nanoclusters, and the amelioration of oncogenic Ras-dependent signaling and hyperproliferation *in vivo*.

Long chain n-3 PUFA modify oncogenic KRas proteolipid nanoassembly composition.

We next sought to determine the mechanism by which n-3 PUFA disrupt cholesterol-dependent and independent lateral segregation resulting in a reduction in ERK signaling. Since recruitment of the effector Raf to active Ras proteolipid assemblies is a requirement of the RAS/ERK signal cascade, this effector recruitment can be monitored by co-expression of full length activated KRasG12V with the Ras-binding domain (RBD) of the effector C-Raf[6]. Similar to previous experiments, YAMC cells were treated with PUFA (50 µM) for 72 h. EPA and DHA reduced the FRET signal between full length active KRasG12V and the RBD, while LA had no effect compared to untreated control (**Figure 5A & B**). The dose-dependent effect of DHA on the suppression of Raf effector recruitment is shown in **Figure 5C &D**.

Raf effectors contain lipid binding domains that drive interactions with specific lipids, such as phosphatidylserine (PS) and phosphatidic acid (PA)[43,44]. Active KRas proteolipid complexes concentrate specific lipids (PA & PS) and segregate others (cholesterol) in order to facilitate efficient effector recruitment and therefore signal transduction[9,36,45,46]. Thus, we assessed the effects of n-3 PUFA on the lipid composition of oncogenic KRas proteolipid assemblies using FLIM-FRET in YAMC cells transiently co-expressing full length activated KRasG12V and fluorescently tagged lipid binding domains for PS (LactC2-RFP) or PA (Spo20-RFP). None of the fatty acid treatments tested had an effect on the interaction of PS with KRasG12V (**Figure 5E & F**). In contrast, EPA and DHA reduced the interaction of PA

with KRasG12V (**Figure 5G & H**). Importantly, addition of exogenous PA but not PS to DHA treated cells restored oncogenic KRasG12V-mediated RBD recruitment (**Figure 5I**).

KRasG12V is typically not localized to cholesterol-rich domains, as these domains are suboptimal for Raf activation[36,46]. Thus, it is noteworthy that DHA increased the association of KRasG12V with the cholesterol marker D4H (**Figure 5J & K**). These data suggest that DHA treatment mislocalizes activated KRasG12V into a cholesterol-rich domain, which likely contains inactivated H-Ras (**Figure 2I**). Furthermore, in DHA treated cells, exogenous PA restored the lateral segregation of KRasG12V away from the cholesterol marker D4H, while PS only partially rescued the structural organization of the membrane (**Figure 5K**). Interestingly, incubation of DHA treated cells with either PA or PS failed to restore the lateral segregation of KRasG12V and the cholesterol-dependent tH domain (**Figure 5L**). These observations indicate that membrane enrichment of DHA results in the redistribution of PA in the plasma membrane inner leaflet, which in turn disrupts the nanoscale organization and function of oncogenic KRas proteolipid signaling complexes.

Discussion

Here we provide evidence that a diet containing long chain n-3 PUFA, e.g., EPA and DHA, attenuates oncogenic Ras signaling and phenotype (hyperproliferation) by altering its nanoscale proteolipid interactions at the plasma membrane (**Figure 6**). To our knowledge, this is the first *in vivo* evidence that dietary bioactives can fundamentally alter Ras membrane nanoscale organization and signaling in the intestine. This is highly relevant since no curative treatments for KRas-driven cancer are available. From a translational and feasibility perspective, these findings lay the foundation for the development of toxicologically innocuous KRas therapeutic approaches. Our data suggest that membrane therapy as a strategy likely requires the long term shaping of cellular phospholipids and hence their resident proteins[28]. The use of a prolonged regimen as a therapeutic strategy would ideally need to exhibit little or no adverse effects. From a human dose perspective, EPA and DHA administration as high as 17.6 g/day has been shown to be safe and well tolerated[47].

The plasma membrane contains exquisitely organized and compartmentalized signaling domains, composed of lipids and proteins. A combination of complex biophysical (electrostatic and hydrophobic) interactions between multiple lipid species and membrane proteins, drive the formation of these transient signaling domains[48]. With regard to Ras, the highly specific lipid and protein composition of these domains allows selective recruitment of effectors, and

therefore is necessary to maintain efficient signal transduction[49]. With respect to diet, it has been previously demonstrated that the incorporation of long chain n-3 PUFA into phospholipids can affect the biophysical properties of the plasma membrane[50]. Here we extend previous studies focusing on membrane biophysical properties, by addressing the impact of n-3 PUFA on the nanoscale localization of lipids and Ras proteins. The lateral segregation and coalescence of Ras proteolipid complexes is likely driven by similar biophysical properties that govern the phase separation of lipids observed in model membranes[51]. Additionally, the ratios of cholesterol and sphingomyelin influence phase separation[51]. This is relevant because dietary n-3 PUFA reduces colonic caveolae cholesterol[25] and T-cell lipid raft sphingomyelin content[26]. Furthermore, long chain n-3 PUFA stabilizes phase separation of membranes generated *in silico* and in cell culture[35,52]. This effect of n-3 PUFA on phase separation is in part dependent on its mol% enrichment in the membrane[52]. Therefore, the mol% enrichment of n-3 PUFA in plasma membrane phospholipids is critical to our mechanistic hypothesis. The dose of n-3 PUFA used in our mouse studies is a human equivalent dose of approximately 8.6 g/day, based on body surface area[53]. Thus, the mol% enrichment of total n-3 PUFA observed in both our mouse and *Drosophila* models (**Figure 1B** and **Table 1**) is physiologically attainable in humans[47]. These studies suggest that the biophysical effects of n-3 PUFA on the plasma membrane may contribute to alterations in Ras lateral segregation in human subjects.

The spatial organization of Ras isoforms into non-overlapping nanometer scale domains on the plasma membrane facilitates the recruitment of Raf leading to ERK activation[6], thus creating a novel drug target[8]. We observed that long chain n-3 PUFA selectively generate mixed cholesterol-dependent (tH-GFP) and independent (tK-GFP) nanoclusters (**Figure 2G and Figure 4E**). This result is similar to the ability of nonsteroidal anti-inflammatory drugs[7] or actin disruption[10] to generate heterotypic mixed clusters. Interestingly, DHA is known to affect actin dynamics[32,50,54], which may partially explain the mechanism underlying the formation of

heterotypic clusters. Furthermore, the lipid composition of caveolae, which also regulates Ras lateral segregation[55], is modified by long chain n-3 PUFA[25]. Select phospholipid pools such as PS, PA, and phosphatidylinositol-4,5-bisphosphate (PIP_2) are key structural components of Ras nanoclusters[9,10], and the lateral segregation and heterotypic mixing of H- and KRas is dependent on PS levels in the plasma membrane[10]. Interestingly, we have previously demonstrated that dietary fish oil results in the incorporation of EPA and DHA into the acyl chains of PS and to a lesser extent PIP_2[25,26,54]. This is noteworthy, because KRas plasma membrane localization and nanoclustering requires specific PS acyl chain species[11], raising the possibility that the altered PS acyl chain profile generated by dietary fish oil may underlie its effects on Ras nanoclustering.

The recruitment of Raf to KRas nanoclusters requires the acidic lipids PA and PS[43,44]. We demonstrate that n-3 PUFA mislocalizes activated KRas to membrane microdomains depleted of PA (**Figure 5H**). Notably, the mislocalized KRas predominantly associates with cholesterol-rich domains (**Figure 5K**) containing truncated HRas (**Figure 2I**). Cholesterol-rich regions of the membrane are suboptimal for Raf activation[36,46], therefore these perturbations result in the failed recruitment of Raf to activated KRas proteolipid assemblies (**Figure 5B & C**) and the attenuation of ERK signaling (**Figure 3 and Figure 4H**). Importantly, PA mediated signaling is required for the nuclear activation of ERK[40]. Interestingly, exogenous supplementation of PA to DHA treated cells restores KRasG12V and cholesterol lateral segregation (**Figure 5K**), and Raf recruitment (**Figure 5I**), without restoring KRasG12V and tH segregation (**Figure 5L**). These findings suggest that the heterotypic clustering of KRasG12V and tH does not contribute to the anti-proliferative effect of n-3 PUFA. Instead, our data support a mechanistic model in which activated KRas must be associated with a pool of PA in a cholesterol-poor domain of the membrane in order to recruit Raf and propagate signaling (**Figure 6**). Further research is

required to elucidate how exogenous PA can reshape DHA modified KRas proteolipid complexes.

While cholesterol is the predominant sterol present in mammalian plasma membranes, ergosterol is the major sterol component present in lower eukaryotes such as *Drosophila*[21]. This suggests an evolutionary conserved aspect of membrane organization that even extends to the neural system[18]. Therefore, our results using cholesterol-sensitive and insensitive Ras constructs are interpretable in the *Drosophila* ISC model (**Figure 4C-E**). In this in vivo study, we also utilized a functionally active mutated form of Ras1 (RasV12). Interestingly, long chain n-3 PUFA suppressed Ras1-dependent oncogenic signaling and phenotypes in the fly (**Figure 4F-H**), similar to the murine model (**Figure 1**). We, therefore, posit that long-chain n-3 PUFA may also alter the nanoscale organization of *Drosophila* Ras1 proteolipid complexes, similar to mammalian KRas (**Figure 6**). However, further work is needed to address this possibility.

In conclusion, our findings mechanistically link the reshaping of Ras proteolipid composition with the ability of n-3 PUFA to attenuate oncogenic Ras driven colonic hyperproliferation. We propose that our novel observations support the feasibility of utilizing dietary strategies that target plasma membrane organization to reduce Ras oncogenic signaling and cancer risk[28].

Acknowledgements

We thank J.F. Hancock (UT Health Science Center Houston, TX) for providing transgenic flies carrying UAS expression constructs GPF-tH, RFP-tH, GFP-tK and RFP-tK; Dr Guangwei Du (UT Health Science Center Houston, TX) for providing the Spo20-RFP plasmid and Dr. Gregory Fairn (University of Toronto, Canada) for providing the D4H-RFP plasmid. mRFP-Lact-C2 was a gift from Sergio Grinstein (Addgene plasmid # 74061), and mRFP-RBD(R59A)-mRFP was a gift from Karel Svoboda (Addgene plasmid # 18664). We also thank Shigeo Hayashi (Riken Center for Development Biology, Japan) for providing the esg-Gal4 construct and Eric Fearon (Department of Internal Medicine, University of Michigan) for generously donating CDX2P^{creERT}, LSL-K-Ras G12D compound mice, and Ms. Rachel Wright for generating the summary diagram. This work was supported by National Institutes of Health grants R35CA197707 and P30ES023512 and funds from the Allen Endowed Chair in Nutrition & Chronic Disease Prevention. Natividad Fuentes is a recipient of a Predoctoral Fellowship in Pharmacology/Toxicology from the PhRMA Foundation and the National Science Foundation

Texas A&M University System Louis Stokes Alliance for Minority Participation (TAMUS LSAMP) Bridge to the Doctorate Fellowship (HRD-1249272).

Author Contributions

Conceptualization, N.R.F. and R.S.C.; Methodology, M.M., P.H., T.S., S. B., and J.K.; Investigation, N.R.F., M.M., R.B. and Y.F.; Writing – Original Draft, N.R.F. and R.S.C.; Writing – Review & Editing, N.R.F. M.M., R.B., P.H., T.S., S. B, I.P., J.K. and R.S.C.; Funding Acquisition, R.S.C.; Resources, S.B. and I.P.; Supervision, J.K., and R.S.C.

References

1. Cox, A. D., Fesik, S. W., Kimmelman, A. C., Luo, J. & Der, C. J. Drugging the undruggable RAS: Mission Possible? *Nat. Rev. Drug Discov.* **13,** 828–51 (2014).

2. Stephen, A. G., Esposito, D., Bagni, R. K. & McCormick, F. Dragging ras back in the ring. *Cancer Cell* **25,** 272–281 (2014).

3. Phipps, A. I. *et al.* KRAS-mutation status in relation to colorectal cancer survival: the joint impact of correlated tumour markers. *Br J Cancer* **108,** 1757–1764 (2013).

4. Herrmann, C. Ras-effector interactions: after one decade. *Curr. Opin. Struct. Biol.* **13,** 122–9 (2003).

5. Downward, J. Targeting RAS signalling pathways in cancer therapy. *Nat Rev Cancer* **3,** 11–22 (2003).

6. Tian, T. *et al.* Plasma membrane nanoswitches generate high-fidelity Ras signal transduction. *Nat Cell Biol* **9,** 905–914 (2007).

7. Zhou, Y., Cho, K.-J., Plowman, S. J. & Hancock, J. F. Nonsteroidal anti-inflammatory drugs alter the spatiotemporal organization of Ras proteins on the plasma membrane. *J. Biol. Chem.* **287,** 16586–95 (2012).

8. Cho, K.-J. J. K. & Hancock, J. F. J. F. Ras nanoclusters: a new drug target? *Small GTPases* **4,** 57–60 (2013).

9. Zhou, Y. & Hancock, J. F. in *Advances in Biomembranes and Lipid Self-Assembly* **25,** 41–62 (2017).

10. Zhou, Y. *et al.* Signal integration by lipid-mediated spatial cross talk between Ras nanoclusters. *Mol Cell Biol* **34,** 862–876 (2014).

11. Zhou, Y. *et al.* Lipid-Sorting Specificity Encoded in K-Ras Membrane Anchor Regulates Signal Output. *Cell* **168,** 239–251.e16 (2017).

12. Chapkin, R. S., Akoh, C. C. & Miller, C. C. Influence of dietary n-3 fatty acids on macrophage glycerophospholipid molecular species and peptidoleukotriene synthesis. *J Lipid Res* **32,** 1205–1213 (1991).

13. Hall, M. N., Chavarro, J. E., Lee, I.-M. M., Willett, W. C. & Ma, J. A 22-year prospective study of fish, n-3 fatty acid intake, and colorectal cancer risk in men. *Cancer Epidemiol Biomarkers Prev* **17,** 1136–1143 (2008).

14. Lien, E. L. Toxicology and safety of DHA. *Prostaglandins Leukot Essent Fat. Acids* **81,** 125–132 (2009).

15. Feng, Y. *et al.* Sox9 induction, ectopic paneth cells, and mitotic spindle axis defects in mouse colon adenomatous epithelium arising from conditional biallelic Apc inactivation. *Am. J. Pathol.* **183,** 493–503 (2013).

16. Kim, E. *et al.* Rapidly cycling Lgr5+ stem cells are exquisitely sensitive to extrinsic dietary factors that modulate colon cancer risk. *Cell Death Dis.* **7,** e2460 (2016).

17. Habets, G. G. *et al.* cDNA array analyses of K-ras-induced gene transcription. *Methods Enzymol.* **332,** 245–60 (2001).

18. Zhou, Y. *et al.* SIGNAL TRANSDUCTION. Membrane potential modulates plasma membrane phospholipid dynamics and K-Ras signaling. *Science* **349,** 873–6 (2015).

19. Piper, M. D. W. *et al.* A holidic medium for Drosophila melanogaster. *Nat. Methods* **11,** 100–5 (2014).

20. Shen, L. R. *et al.* Drosophila lacks C20 and C22 PUFAs. *J. Lipid Res.* **51,** 2985–92 (2010).

21. Carvalho, M. *et al.* Effects of diet and development on the Drosophila lipidome. *Mol. Syst. Biol.* **8,** 600 (2012).

22. Jiang, H., Grenley, M. O., Bravo, M.-J., Blumhagen, R. Z. & Edgar, B. A. EGFR/Ras/MAPK signaling mediates adult midgut epithelial homeostasis and regeneration in Drosophila. *Cell Stem Cell* **8,** 84–95 (2011).

23. Chang, C., Sud, D. & Mycek, M. in *Methods in cell biology* **81,** 495–524 (2007).

24. Najumudeen, A. K. *et al.* Cancer stem cell drugs target K-ras signaling in a stemness context. *Oncogene* **35,** 5248–5262 (2016).

25. Ma, D. W. L. *et al.* n-3 PUFA alter caveolae lipid composition and resident protein localization in mouse colon. *FASEB J* **18,** 1040–1042 (2004).

26. Fan, Y. Y., McMurray, D. N., Ly, L. H. & Chapkin, R. S. Dietary (n-3) polyunsaturated fatty acids remodel mouse T-cell lipid rafts. *J Nutr* **133,** 1913–1920 (2003).

27. Turk, H. F., Barhoumi, R. & Chapkin, R. S. Alteration of EGFR spatiotemporal dynamics suppresses signal transduction. *PLoS One* **7,** e39682 (2012).

28. Fuentes, N. R., Salinas, M. L., Kim, E. & Chapkin, R. S. Emerging role of chemoprotective agents in the dynamic shaping of plasma membrane organization. *Biochim. Biophys. Acta* **1859,** 1668–1678 (2017).

29. Kim, W. *et al.* Regulatory activity of polyunsaturated fatty acids in T-cell signaling. *Prog Lipid Res* **49,** 250–261 (2010).

30. Chapkin, R. S., Wang, N., Fan, Y.-Y., Lupton, J. R. & Prior, I. A. Docosahexaenoic acid alters the size and distribution of cell surface microdomains. *Biochim. Biophys. Acta - Biomembr.* **1778,** 466–471 (2008).

31. Prior, I. A., Muncke, C., Parton, R. G. & Hancock, J. F. Direct visualization of Ras proteins in spatially distinct cell surface microdomains. *J Cell Biol* **160,** 165–170 (2003).

32. Turk, H. F. *et al.* Inhibitory effects of omega-3 fatty acids on injury-induced epidermal growth factor receptor transactivation contribute to delayed wound healing. *Am J Physiol Cell Physiol* **304,** C905-17 (2013).

33. Seo, J., Barhoumi, R., Johnson, A. E., Lupton, J. R. & Chapkin, R. S. Docosahexaenoic acid selectively inhibits plasma membrane targeting of lipidated proteins. *FASEB J* **20,** 770–772 (2006).

34. Conquer, J. A. & Holub, B. J. Effect of supplementation with different doses of DHA on the levels of circulating DHA as non-esterified fatty acid in subjects of Asian Indian background. *J Lipid Res* **39,** 286–292 (1998).

35. Levental, K. R. *et al.* Polyunsaturated Lipids Regulate Membrane Domain Stability by Tuning Membrane Order. *Biophys. J.* **110,** 1800–1810 (2016).

36. Prior, I. A. *et al.* GTP-dependent segregation of H-ras from lipid rafts is required for biological activity. *Nat. Cell Biol.* **3,** 368–375 (2001).

37. Stolze, B., Reinhart, S., Bulllinger, L., Fröhling, S. & Scholl, C. Comparative analysis of KRAS codon 12, 13, 18, 61, and 117 mutations using human MCF10A isogenic cell lines. *Sci. Rep.* **5,** 8535 (2015).

38. Prior, I. A., Lewis, P. D. & Mattos, C. A comprehensive survey of Ras mutations in cancer. *Cancer Res* **72,** 2457–2467 (2012).

39. Brunet, A. *et al.* Nuclear translocation of p42/p44 mitogen-activated protein kinase is required for growth factor-induced gene expression and cell cycle entry. *EMBO J.* **18,** 664–674 (1999).

40. Zhang, F. *et al.* Temporal production of the signaling lipid phosphatidic acid by phospholipase D2 determines the output of extracellular signal-regulated kinase signaling in cancer cells. *Mol Cell Biol* **34,** 84–95 (2014).

41. Biteau, B., Hochmuth, C. E. & Jasper, H. Maintaining Tissue Homeostasis: Dynamic Control of Somatic Stem Cell Activity. *Cell Stem Cell* **9,** 402–411 (2011).

42. Jiang, H. & Edgar, B. A. EGFR signaling regulates the proliferation of Drosophila adult

midgut progenitors. *Development* **136,** 483–93 (2009).

43. Ghosh, S., Strum, J. C., Sciorra, V. A., Daniel, L. & Bell, R. M. Raf-1 kinase possesses distinct binding domains for phosphatidylserine and phosphatidic acid. Phosphatidic acid regulates the translocation of Raf-1 in 12-O-tetradecanoylphorbol-13-acetate-stimulated Madin-Darby canine kidney cells. *J. Biol. Chem.* **271,** 8472–80 (1996).

44. Ghosh, S. *et al.* The cysteine-rich region of raf-1 kinase contains zinc, translocates to liposomes, and is adjacent to a segment that binds GTP-ras. *J. Biol. Chem.* **269,** 10000–7 (1994).

45. Zhou, Y. & Hancock, J. F. Ras nanoclusters: Versatile lipid-based signaling platforms. *Biochim. Biophys. Acta* **1853,** 841–849 (2015).

46. Inder, K. *et al.* Activation of the MAPK Module from Different Spatial Locations Generates Distinct System Outputs. *Mol. Biol. Cell* **19,** 4776–4784 (2008).

47. Skarke, C. *et al.* Bioactive products formed in humans from fish oils. *J. Lipid Res.* **56,** 1808–20 (2015).

48. Sezgin, E., Levental, I., Mayor, S. & Eggeling, C. The mystery of membrane organization: composition, regulation and roles of lipid rafts. *Nat. Rev. Mol. Cell Biol.* **18,** 361–374 (2017).

49. Zhou, Y. & Hancock, J. F. Deciphering lipid codes: K-Ras as a paradigm. *Traffic* (2017). doi:10.1111/tra.12541

50. Kim, W. *et al.* n-3 polyunsaturated fatty acids suppress the localization and activation of signaling proteins at the immunological synapse in murine CD4+ T cells by affecting lipid raft formation. *J Immunol* **181,** 6236–6243 (2008).

51. Veatch, S. L. & Keller, S. L. Separation of Liquid Phases in Giant Vesicles of Ternary Mixtures of Phospholipids and Cholesterol. *Biophys. J.* **85,** 3074–3083 (2003).

52. Fan, Y.-Y. *et al.* Remodelling of primary human CD4+ T cell plasma membrane order by n-3 PUFA. *Br. J. Nutr.* 1–13 (2017). doi:10.1017/S0007114517003385

53. Reagan-Shaw, S., Nihal, M. & Ahmad, N. Dose translation from animal to human studies revisited. *FASEB J* **22,** 659–661 (2008).

54. Hou, T. Y. *et al.* n-3 polyunsaturated fatty acids suppress phosphatidylinositol 4,5-bisphosphate-dependent actin remodelling during CD4+ T-cell activation. *Biochem J* **443,** 27–37 (2012).

55. Ariotti, N. *et al.* Caveolae regulate the nanoscale organization of the plasma membrane to remotely control Ras signaling. *J Cell Biol* **204,** 777–792 (2014).

Tables

Table 1. Incorporation of exogenous fatty acids into *Drosophila* gut membrane phospholipids.

Fatty Acid	Holidic Control	Fish Oil
	(mol%)	(mol%)
14:0	4.62	3.07
16:0	11.62	22.79
16:1n-7	35.68	20.71
18:0	3.36	3.47
18:1n-9	36.77	32.19
18:1n-7	0.00	1.94
18:2n-6 (LA)	3.60	4.73
20:0	3.28	1.77
20:4n-6	0.46	0.00
20:5n-3 (EPA)	0.00	5.47
22:0	0.62	0.80
22:6n-3 (DHA)	0.00	1.12

Values represent means from pooled Drosophila guts (n=51 for Control, n=46 for Fish Oil), grown in two separate vials.

Only selected fatty acids in which at least one observation was > 0.2 mol% are reported.

Figure Legends

Figure 1. Dietary n-3 PUFA ameliorate oncogenic KRasG12D mediated colonic phenotypes. (A) Experimental design to determine the efficacy of dietary intervention on a genetic mouse model of oncogenic KRasG12D driven hyper-proliferation in the colon. (B) Isolated colonic crypt phospholipid profile from mice fed the experimental diets. (C) Alcian blue-staining of colonic crypts, including high magnification of crypts in dashed black box, with red dashed arrow representing crypt length. (D) Nuclei (blue) and EdU-labeled (red) proliferating colonocytes in mice 4 weeks post tamoxifen (Tam, 200 mg/kg) fed corn or fish oil-containing diets. High magnification of crypts is shown in each dashed white box. Quantitative analysis of (E) crypt length and (F) cell proliferation. Scale bar = 50 µm. Statistical significance between treatments as indicated by different letters ($P<0.05$) was examined using one-way ANOVA and uncorrected Fisher's LSD tests (Panel E; n = 4 mice per group and at least 508 crypts counted; Panel F; n = 4 mice per group and 200 crypts counted). LA – linoleic acid, EPA – eicosapentaenoic acid, DHA – docosahexaenoic acid.

Figure 2. Long chain n-3 PUFA disrupt Ras spatiotemporal dynamics. Nanoclustering-FRET analysis (illustrated in schemes) in (A) YAMC cells co-expressing GFP- and RFP-tagged (B) truncated KRas (tK), (D) truncated HRas (tH), (F) tH-GFP and tK-RFP, or (H) full length oncogenic KRasG12V-GFP and tH-RFP. (A) Representative examples of FLIM-FRET images of YAMC cells from the different FRET samples as indicated. High magnification of cells is shown in each dashed white box. (C, E, G and I) YAMC cells were treated with mevastatin (Mev, 5 μM) or indicated fatty acids (50 μM) for 24 or 72 h, respectively. Cells were transfected 48 h prior to imaging. In all graphs (C, E, G, and I), the apparent FRET efficiency was calculated from FLIM data (mean ± SEM, n= 2-3 independent experiments). Values in the bars indicate the number of cells examined. Statistical significance between treatments as indicated by different letters ($P<0.05$) was examined using one-way ANOVA and uncorrected Fisher's LSD tests. Un – untreated cells, LA – linoleic acid, EPA – eicosapentaenoic acid, DHA – docosahexaenoic acid, Mev – mevalonic acid.

Figure 3. Long chain n-3 PUFA attenuate Ras mediated ERK signaling. (A) SW48-KRasG12D or (C) DKOB8 cells were grown in 8-well glass bottom dishes and treated with 50 μM indicated fatty acid for 72 h. (A) SW48-KRasG12D cells were serum starved (0% FBS) over the final 18 h in the presence of fatty acid and stimulated with EGF (25 ng/ml) for 5 min, then immediately fixed in ice cold 100% methanol. (C) DKOB8 cells were incubated with ponasterone A (10 μM) for the final 48 h, and were serum starved (0% FBS) over the final 18 h in the presence of fatty acid and ponasterone A, then immediately fixed in ice cold 100% methanol. Masked images of pERK (A) +/- EGF or (C) +/- ponasterone A. Scale bar = 20 μm. (B, D) Average fluorescence intensity for pERK. Data represent average fluorescence intensity from at least 10 fields of view with ~10-30 cells per field, from 3 independent experiments. (E) Representative immunofluorescence confocal images of DKOB8 cells stained for pERK (red) and nuclei (blue). (F) Quantification of the ratio of fluorescence intensity of pERK in the nucleus vs cytoplasm. Data represent average fluorescence intensity ratio of nucleus to cytoplasm for at least 90 cells, from 3 independent experiments. Statistical significance between treatments as indicated by different letters ($P<0.05$) was examined using one-way ANOVA and uncorrected Fisher's LSD tests. Un – untreated cells, LA – linoleic acid, EPA – eicosapentaenoic acid, DHA – docosahexaenoic acid, Mev – mevalonic acid.

Figure 4. Dietary n-3 PUFA disrupt Ras spatiotemporal dynamics, suppressing oncogenic Ras driven hyperproliferation phenotype and signaling in *Drosophila* midguts. (A) Schematic diagram of *Drosophila* intestine. (B) Representative intensity and lifetime field of view (FOV) images of *Drosophila* midguts. Nanoclustering-FRET analysis (illustrated in schemes) in *Drosophila* midgut stem cells co-expressing GFP- and RFP-tagged (C) truncated K-Ras (tK), (D) truncated H-Ras (tH) or (E) tH-GFP and tK-RFP. (C, D, and E) 1-2 d old *Drosophila* were placed on holidic diet containing no lipid (red) or fish oil (purple) for 5 d prior to dissection and mounting of midguts for microscopy. In all graphs (C, D and E), the apparent FRET efficiency was calculated from FLIM data (mean ± SEM, n=2 independent experiments). Values in the bars indicate the number of analyzed FOVs. Induction of oncogenic RasV12 in *Drosophila* midgut stem cells resulted in (F) hyperproliferation at 24 h and luminal thickening at 48 h. *Drosophila* fed a fish oil vs control holidic diet for 5 d prior to induction of oncogenic RasV12 in midgut stem cells exhibited reduced hyperproliferation and midgut luminal thickening. (G) Quantitative analysis of proliferation as assessed by pH3 at 48 h post RasV12 induction. (H) After 24 h RasV12 induction, guts were harvested and used to assess pERK by western blot. Statistical significance between treatments as indicated by different letters ($P<0.05$) was examined using an unpaired t-test.

Figure 5. Long chain n-3 PUFA alter oncogenic KRasG12V proteolipid composition.

Nanoclustering-FRET analysis (illustrated in scheme) in YAMC cells co-expressing full length oncogenic KRasG12V-GFP and (A) Raf-(R59A)-RBD-RFP, (E) LactC2-RFP, (G) Spo20-RFP, or (J) D4H-RFP. YAMC cells were transfected with KRasG12V-GFP (Donor) alone or co-transfected with indicated RFP tagged probe (Acceptor), and after 48 h fixed in 4% PFA. Where indicated, cells were untreated or treated with indicated fatty acid (50 μM) for 72 h and 100 μM phosphatidic acid (PA, 18:0-18:1, Avanti #840861) or phosphatidylserine (PS, 18:0-18:1, Avanti #840039) for 45 min prior to fixation. Values in the bars indicate the number of cells examined. (D) Representative examples of FLIM-FRET images of YAMC cells from the different FRET samples as indicated. High magnification of cells is shown in each dashed white box. Statistical significance between treatments as indicated by different letters ($P<0.05$) was examined using one-way ANOVA and uncorrected Fisher's LSD tests. Un – untreated cells, LA – linoleic acid, EPA – eicosapentaenoic acid, DHA – docosahexaenoic acid, Mev – mevalonic acid.

Figure 6. Summary diagram highlighting n-3 PUFA suppression of oncogenic Ras mediated signaling and hyperproliferation via disruption of Ras nanoscale proteolipid composition. (A) Incorporation of long chain n-3 PUFA into colonocyte plasma membrane phospholipids mislocalizes oncogenic KRas from PA-rich domains into cholesterol-rich but PA-poor domains, generating heterotypic mixed clusters of tH and KRas proteins, thereby disrupting its ability as a nanoswitch to regulate ERK signaling. This results in the suppression of oncogenic Ras-driven phenotypes in the colon. (B) Exogenous PA restores the lateral segregation of oncogenic KRas from cholesterol-rich domains and the recruitment of Raf.

Figure 1

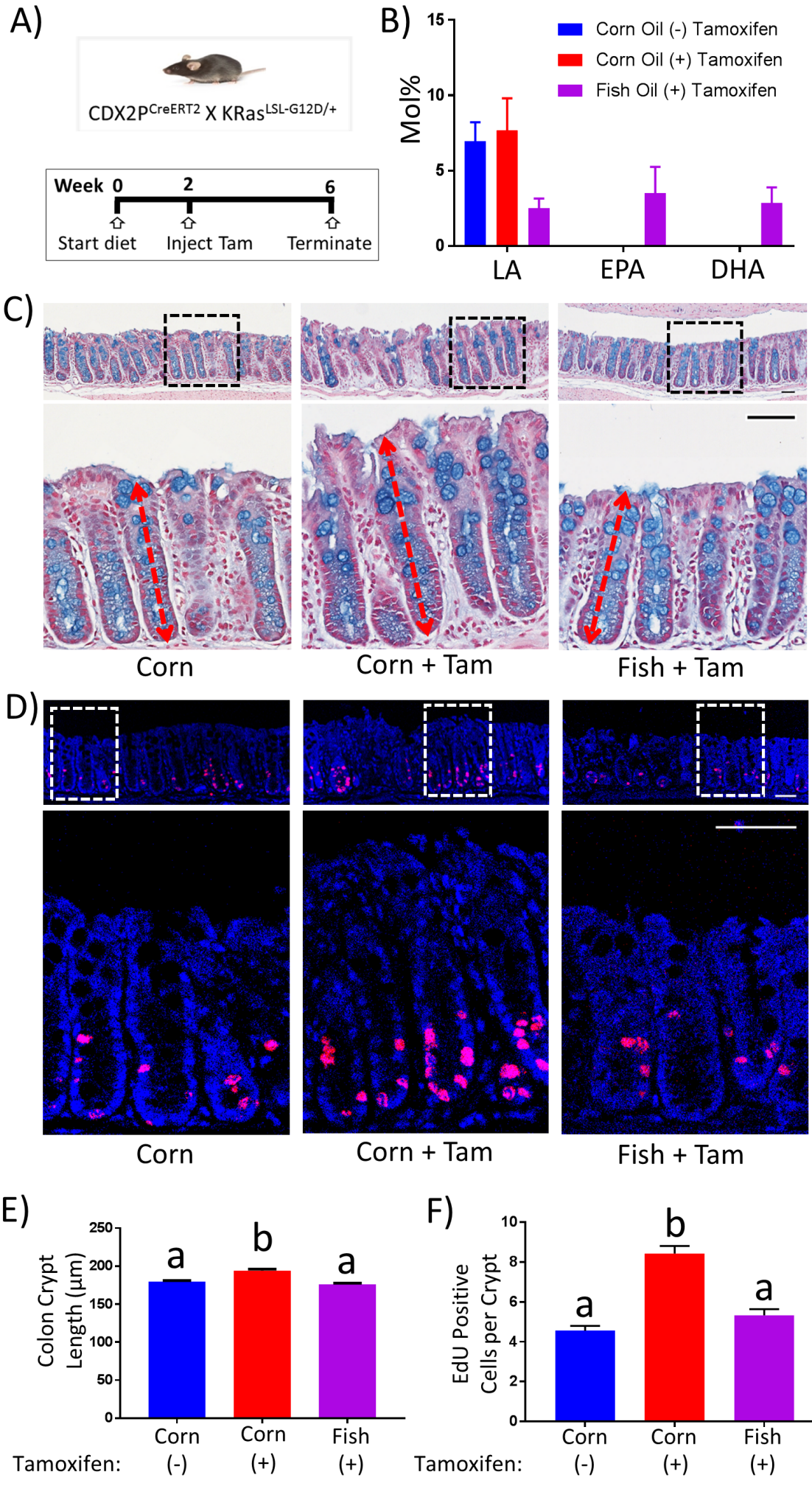
A)
CDX2P^CreERT2 X KRas^LSL-G12D/+
Week 0
2
6
Start diet
Inject Tam
Terminate
B)
Corn Oil (-) Tamoxifen
Corn Oil (+) Tamoxifen
Fish Oil (+) Tamoxifen
Mol%
15
10
5
0
LA
EPA
DHA
C)
Corn
Corn + Tam
Fish + Tam
D)
Corn
Corn + Tam
Fish + Tam
E)
Colon Crypt Length (µm)
250
200
150
100
50
0
a
b
a
Corn (-)
Corn (+)
Fish (+)
Tamoxifen:
F)
EdU Positive Cells per Crypt
10
8
6
4
2
0
a
b
a
Corn (-)
Corn (+)
Fish (+)
Tamoxifen:

Figure 2

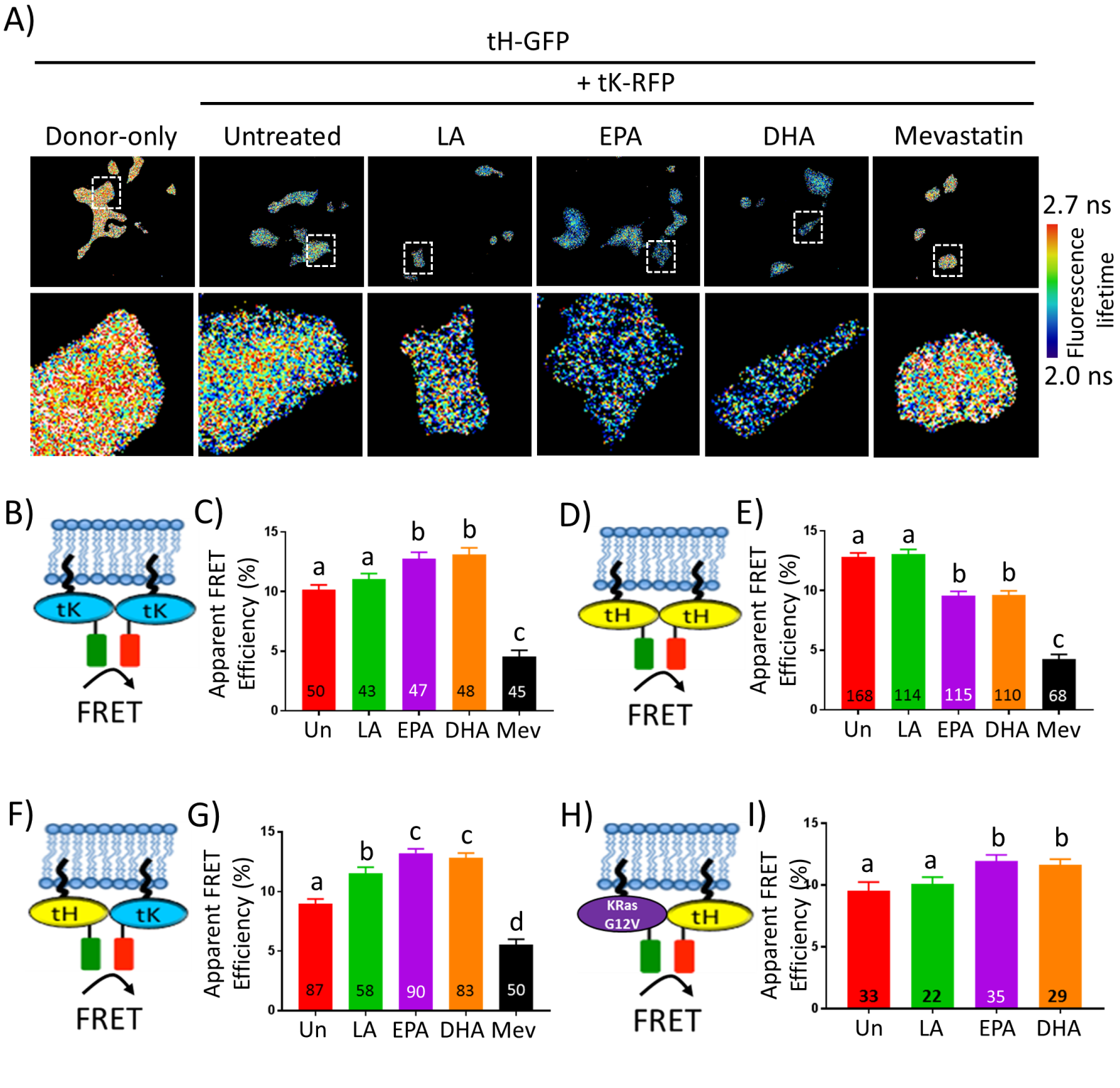
A)
tH-GFP
+ tK-RFP
Donor-only
Untreated
LA
EPA
DHA
Mevastatin
2.7 ns
Fluorescence lifetime
2.0 ns
B)
tK
tK
FRET
C)
Apparent FRET Efficiency (%)
a
a
b
b
c
50
43
47
48
45
Un
LA
EPA
DHA
Mev
D)
tH
tH
FRET
E)
168
114
115
110
68
F)
tH
tK
FRET
G)
87
58
90
83
50
H)
KRas G12V
tH
FRET
I)
33
22
35
29

Figure 3

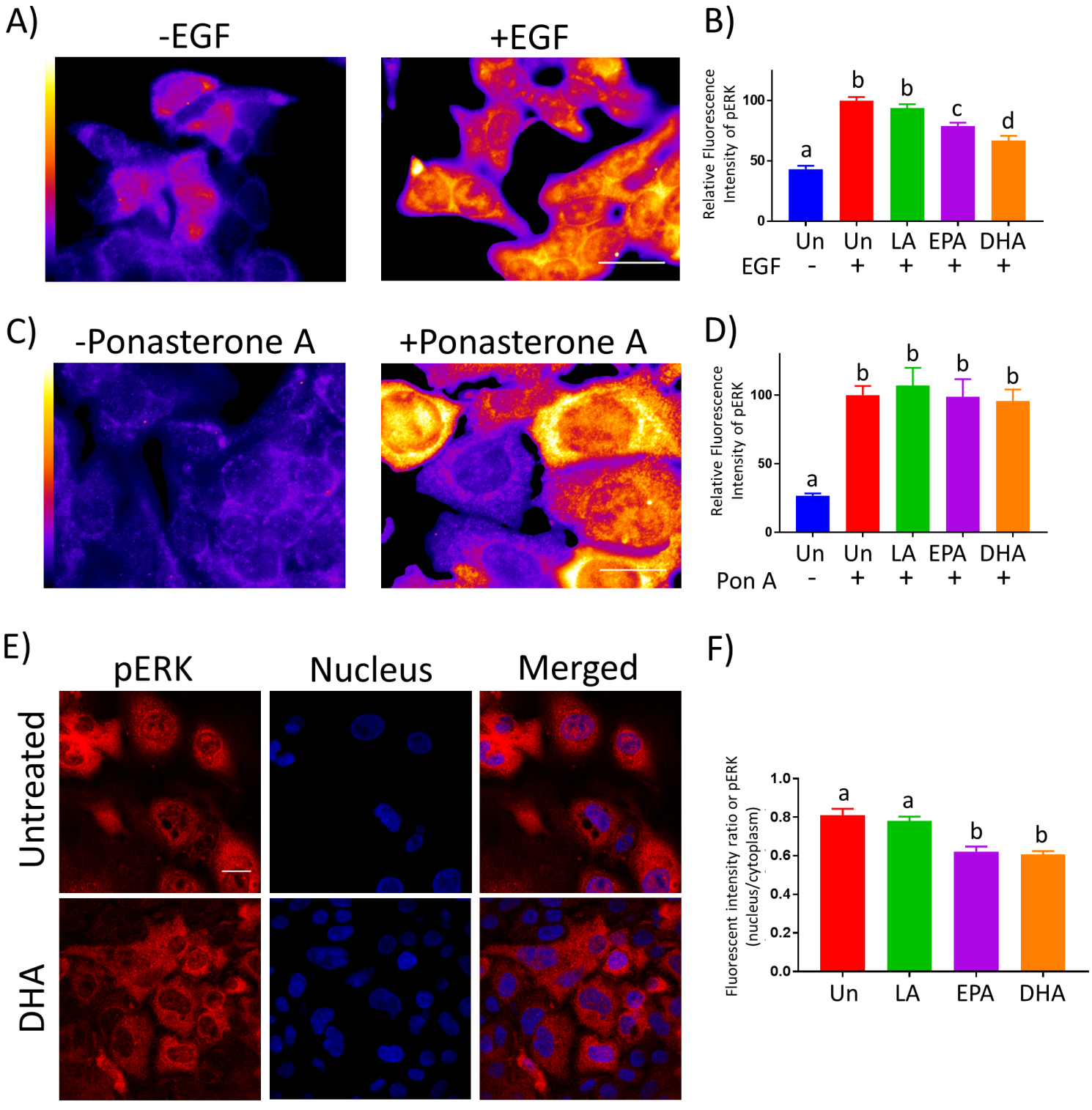
A)
-EGF
+EGF
B)
Relative Fluorescence Intensity of pERK
100
50
0
a
b
b
c
d
Un
Un
LA
EPA
DHA
EGF
-
+
+
+
+
C)
-Ponasterone A
+Ponasterone A
D)
Relative Fluorescence Intensity of pERK
100
50
0
a
b
b
b
b
Un
Un
LA
EPA
DHA
Pon A
-
+
+
+
+
E)
pERK
Nucleus
Merged
Untreated
DHA
F)
Fluorescent intensity ratio or pERK (nucleus/cytoplasm)
1.0
0.8
0.6
0.4
0.2
0.0
a
a
b
b
Un
LA
EPA
DHA

Figure 4

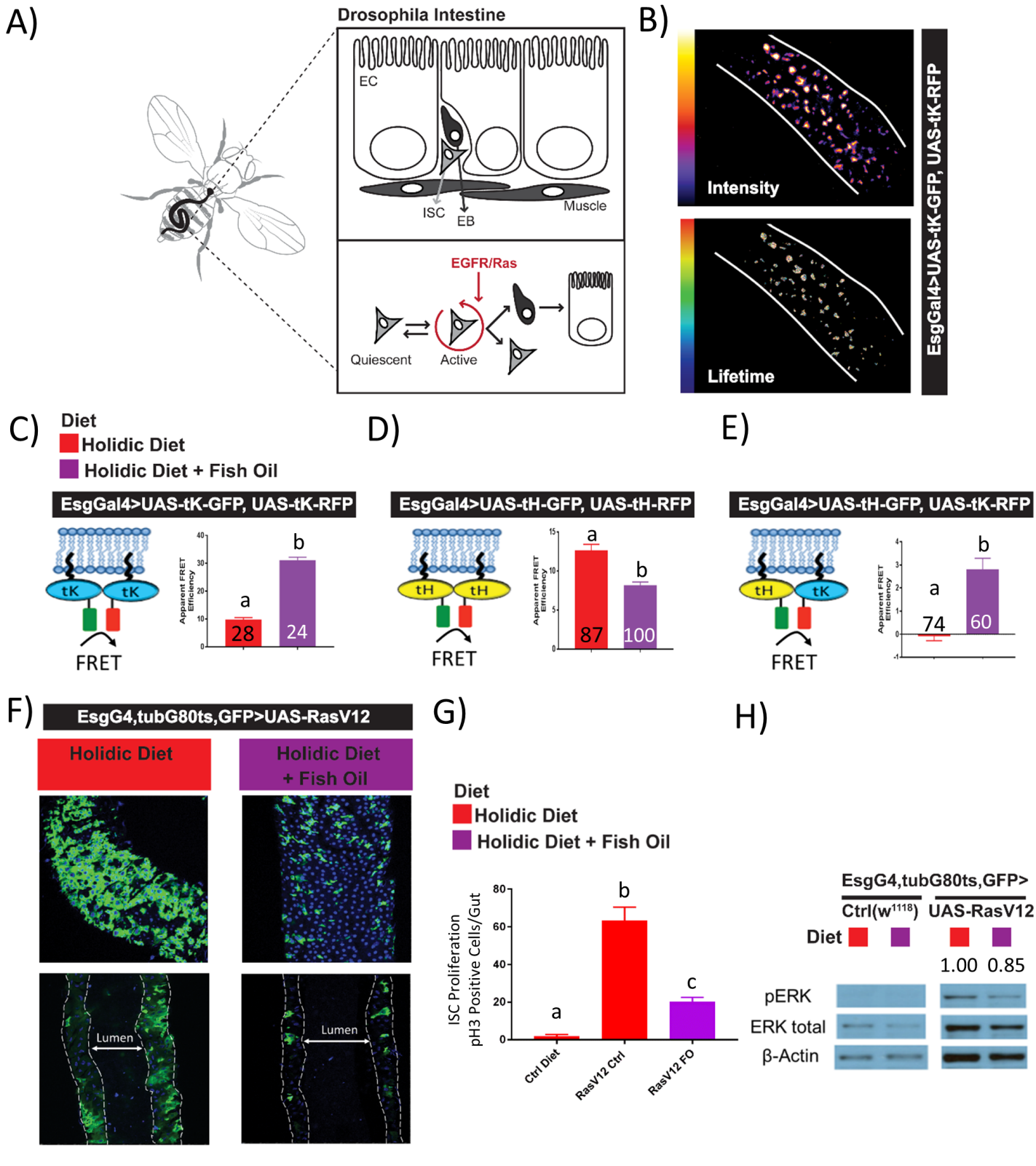
A)
Drosophila Intestine
EC
ISC
EB
Muscle
EGFR/Ras
Quiescent
Active
B)
Intensity
Lifetime
EsgGal4>UAS-tK-GFP, UAS-tK-RFP
C)
Diet
Holidic Diet
Holidic Diet + Fish Oil
EsgGal4>UAS-tK-GFP, UAS-tK-RFP
tK
tK
FRET
Apparent FRET Efficiency
a
b
28
24
D)
EsgGal4>UAS-tH-GFP, UAS-tH-RFP
tH
tH
FRET
Apparent FRET Efficiency
a
b
87
100
E)
EsgGal4>UAS-tH-GFP, UAS-tK-RFP
tH
tK
FRET
Apparent FRET Efficiency
a
b
74
60
F)
EsgG4,tubG80ts,GFP>UAS-RasV12
Holidic Diet
Holidic Diet + Fish Oil
Lumen
Lumen
G)
Diet
Holidic Diet
Holidic Diet + Fish Oil
ISC Proliferation pH3 Positive Cells/Gut
a
b
c
Ctrl Diet
RasV12 Ctrl
RasV12 FO
H)
EsgG4,tubG80ts,GFP>
Ctrl(w1118)
UAS-RasV12
Diet
1.00
0.85
pERK
ERK total
β-Actin

Figure 5

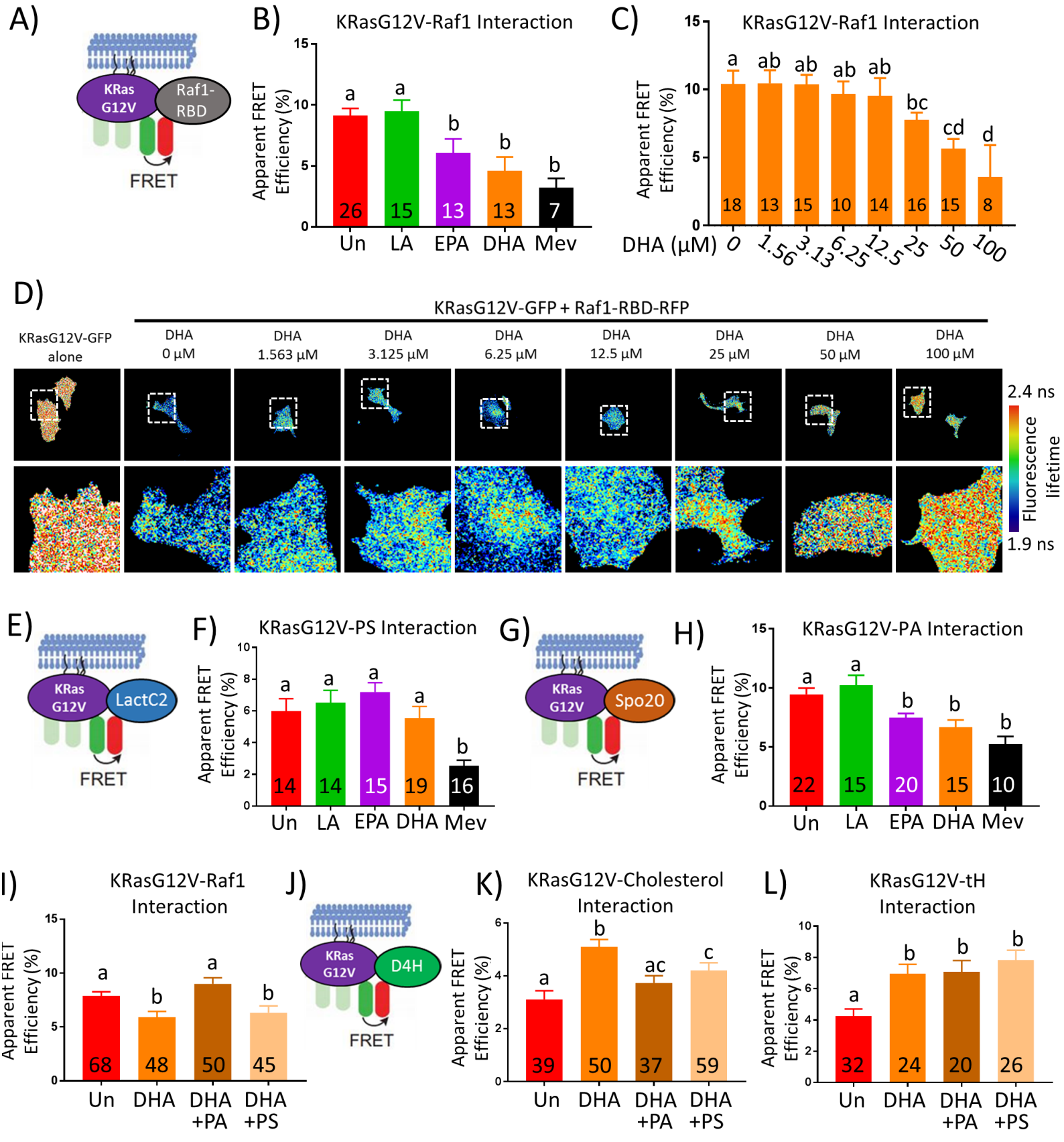
A)
KRas G12V
Raf1-RBD
FRET
B)
KRasG12V-Raf1 Interaction
Apparent FRET Efficiency (%)
Un LA EPA DHA Mev
C)
KRasG12V-Raf1 Interaction
DHA (μM) 0 1.56 3.13 6.25 12.5 25 50 100
D)
KRasG12V-GFP + Raf1-RBD-RFP
KRasG12V-GFP alone
DHA 0 μM
DHA 1.563 μM
DHA 3.125 μM
DHA 6.25 μM
DHA 12.5 μM
DHA 25 μM
DHA 50 μM
DHA 100 μM
2.4 ns
Fluorescence lifetime
1.9 ns
E)
KRas G12V
LactC2
FRET
F)
KRasG12V-PS Interaction
G)
KRas G12V
Spo20
FRET
H)
KRasG12V-PA Interaction
I)
KRasG12V-Raf1 Interaction
Un DHA DHA +PA DHA +PS
J)
KRas G12V
D4H
FRET
K)
KRasG12V-Cholesterol Interaction
L)
KRasG12V-tH Interaction

Figure 6

A)

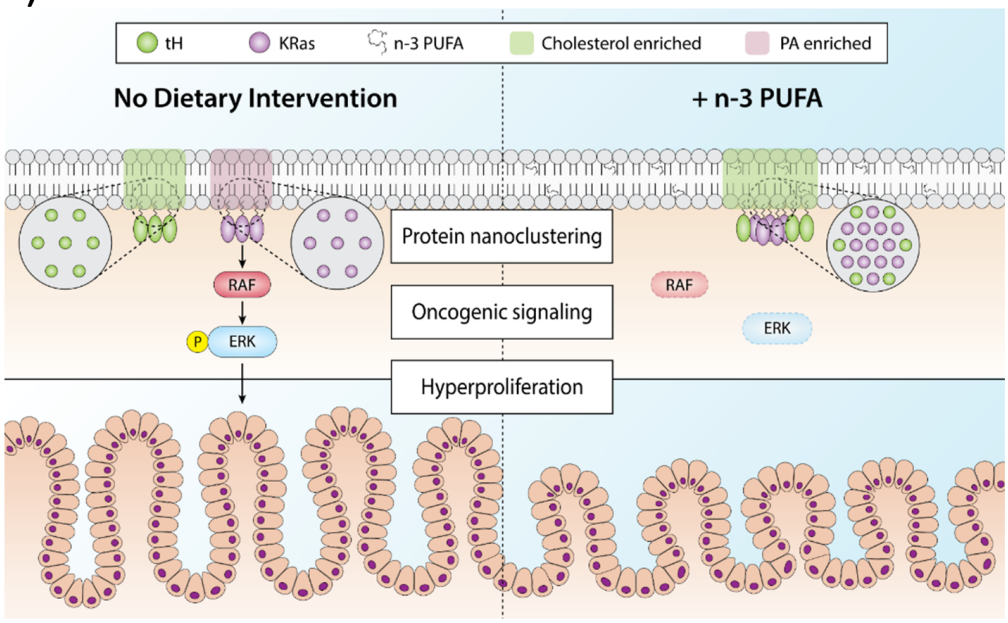
tH
KRas
n-3 PUFA
Cholesterol enriched
PA enriched
No Dietary Intervention
+ n-3 PUFA
Protein nanoclustering
Oncogenic signaling
Hyperproliferation
RAF
P
ERK
RAF
ERK

B)

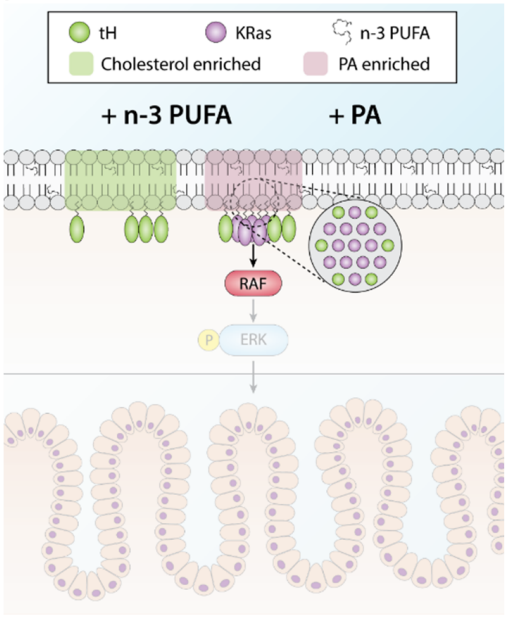
tH
KRas
n-3 PUFA
Cholesterol enriched
PA enriched
+ n-3 PUFA
+ PA
RAF
P
ERK